Catalysis Letters Vol. 104, Nos. 3–4, November 2005 (© 2005)
DOI: 10.1007/s10562-005-7949-5

Preparation of mesoporous Ni–alumina catalyst by one-step sol–gel method: control of textural properties and catalytic application to the hydrodechlorination of *o*-dichlorobenzene

P. Kim, J.B. Joo, H. Kim, W. Kim, Y. Kim, I.K. Song, and J. Yi*

School of Chemical and Biological Engineering, Institute of Chemical Processes, Seoul National University, Shinlim-dong, Kwanak-ku, Seoul, 151-744, Korea

Received 15 April 2005; accepted 23 July 2005

Mesoporous Ni–alumina catalysts (Ni–alumina-pre and Ni–alumina-post) were synthesized by one-step sol–gel method using micelle complex comprising lauric acid and nickel ion as a template with metal source and using aluminum *sec*-butoxide as an aluminum source. The Ni–alumina catalysts showed relatively high surface areas (303 m^2/g for Ni–alumina-pre and 331 m^2/g for Ni–alumina-post) and narrow pore size distributions centered at ca. 4 nm. Highly dispersed Ni particles were observed in the Ni–alumina catalysts (ca. 5.2 nm for Ni–alumina-pre and ca. 6.8 nm for Ni–alumina-post) after reduction at 550 °C, while a catalyst prepared without a template (NiAl-comp) exhibited inferior porosity with large metal particles (ca. 12.3 nm). Mesoporous Ni–alumina catalysts with different porosity were obtained by employing different hydrolysis step of aluminum source. When aluminum source was hydrolyzed under the presence of micelle complex, a supported Ni catalyst with highly developed framework mesoporosity was obtained (Ni–alumina-post). On the other hand, when aluminum source was pre-hydrolyzed followed by mixing with micelle solution, the resulting catalyst (Ni–alumina-pre) retained high portion of textural porosity. It was revealed that the hydrolysis method employed in this research affected not only textural properties but also metal-support interaction in the Ni–alumina catalysts. It was also found that the Ni–alumina-pre catalyst exhibited weaker interaction between nickel and alumina than the Ni–alumina-post, leading to higher degree of reduction in the Ni–alumina-pre catalyst. In the hydrodechlorination of *o*-dichlorobenzene, the Ni–alumina catalysts exhibited better catalytic performance than the NiAl-comp catalyst, which was attributed to higher metal dispersion in the Ni–alumina catalysts. In particular, the Ni–alumina-pre catalyst showing 1.5 times higher degree of reduction and larger amounts of *o*-dichlorobenzene adsorption exhibited better catalytic performance than the Ni–alumina-post catalyst.

KEY WORDS: mesoporous Ni–alumina catalyst; template; one-step sol–gel method; hydrodechlorination; *o*-dichlorobenzene.

1. Introduction

Mesoporous materials prepared by a self-assembled surfactant aggregate have been widely studied and employed in many fields of material science and engineering due to their remarkable properties such as high surface area, large pore volume, and narrow pore size distribution [1–17]. These materials are potentially important as highly efficient catalyst supports because of the merit of controllable porosity that makes supported catalysts have desirable level of diffusion efficiency. Among mesoporous materials, mesoporous alumina has attracted much attention as a catalyst support in the petrochemical industry. Ionic or neutral surfactants have been widely used as chemical templates in the preparation of mesoporous alumina by templating methods [15–19]. It is known that mesoporous aluminas have a three-dimensional interconnected pore system in the form of sponge-like structure, which is a great advantage in the catalytic applications [20–23]. Our research group has prepared pure mesoporous alumina at an ambient temperature and an atmospheric pressure, by reacting an aluminum alkoxide with various carboxylic acids in the presence of controlled amounts of water [5,10,11]. The prepared mesoporous aluminas were found to have high surface area and randomly distributed mesopores with narrow pore size distribution. Even though mesoporous aluminas had high surface area with narrow pore size distribution, nickel catalysts impregnated on mesoporous alumina inevitably experienced pore blocking by metal species during the metal supporting process. This eventually resulted in metal aggregation and low surface area of active metal species [5,24]. One possible route to solve this problem is to co-condensate aluminum precursor with metal source in the presence of template molecules, where the interaction between metal ions and template favorably serves for the formation of highly dispersed metal particles [25].

Most of catalytic reactions that involve the diffusion of reaction species are greatly influenced by the textural properties of the catalyst. It has been claimed that the

* To whom correspondence should be addressed.
E-mail: jyi@snu.ac.kr

textural porosity, resulting from void spaces between primary particles, would be favorable for the introduction of reactant into framework pores, leading to facile diffusion of reactant onto the active sites [26–30]. Therefore, many works have been made on the control of textural porosity of mesoporous materials, especially, for mesoporous silica materials. However, very limited researches on the mesoporous alumina were reported due to the difficulty in controlling the hydrolysis rate of aluminum precursor [26–29].

In this work, we reported the synthesis method of mesoporous Ni–alumina catalyst by one-step sol–gel method and the control methodology of textural porosity by employing different hydrolysis method. The preparation method (one-step sol–gel method) suggested in this research is very efficient for the preparation of highly dispersed Ni catalyst supported on mesoporous alumina because it does not require any additional step for Ni supporting. The prepared mesoporous Ni–alumina catalysts were applied to the model hydrodechlorination reaction of *o*-dichlorobenzene

2. Experimental

2.1. Synthesis of nickel incorporated mesoporous alumina catalysts

Overall schematic for the preparation of Ni–alumina catalysts is shown in figure 1. The Ni–alumina catalysts were synthesized by one-step sol–gel method using Al(*sec*-OBu)$_3$ as an aluminum source and using an assembly of lauric acid and nickel ions as a template with metal source. A typical procedure for the preparation of mesoporous Ni–alumina-post catalyst (12.5 wt% nickel loading in the final form) is as follows. Known amounts of Al(*sec*-BuO)$_3$ (Fluka) and lauric acid mixed with $Ni(NO_3)_2 \cdot 6H_2O$ (Fluka) were separately dissolved in *sec*-butyl alcohol (Fluka), and the two solutions were then mixed. The molar ratio of nickel precursor:aluminum source:lauric acid:butanol was fixed at 0.6:5.0:1.0:54. Small amounts of de-ionized water (the molar ratio of H_2O:Al(*sec*-BuO)$_3$ was 1.0:14) were dropped into the mixture at a rate of 1 mL/min, until green-homogeneous precipitates were formed. The resulting slurry was further stirred for 48 h, and subsequently, it was filtered and dried in air. The crude product was calcined at 550 °C for 12 h with an excess stream of air. The temperature was increased up to 550 °C with a ramping rate of 1 °C/min, and maintained at 550 °C for 12 h to yield the final form. Nickel loading of the Ni–alumina catalyst could be easily controlled by changing the molar ratio of nickel precursor with respect to aluminum source.

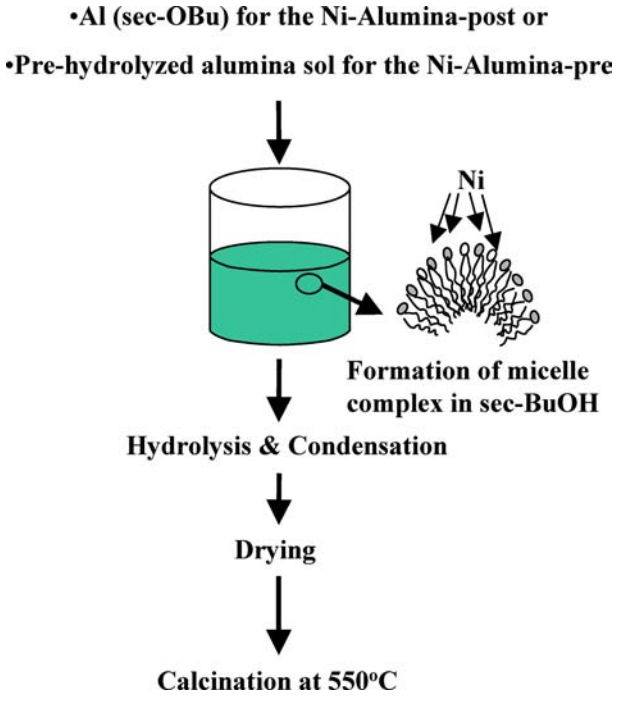

Figure 1. Overall schematic for the preparation of mesoporous Ni–alumina catalysts.

For the preparation of Ni–alumina-pre catalyst, the aluminum precursor was hydrolyzed using 1 M HNO_3 before addition into the butanol solution containing nickel precursor and lauric acid. The molar ratio of nickel precursor, aluminum source, lauric acid, butanol, and water was identical to that used for the preparation of Ni–alumina-post catalyst.

To investigate the effect of template on the properties of the supported Ni catalyst, a nickel catalyst (NiAl-comp) was fabricated without template (lauric acid). The molar ratio of nickel precursor and solvents was almost the same with that used for the preparation of mesoporous Ni–alumina catalysts.

2.2. Characterization

X-ray diffraction (XRD, M18XHF-SRA, MAC/Science) measurements were carried out in order to investigate the phase transformation of support and catalysts. Nitrogen adsorption isotherms were obtained with an ASAP-2010 (Micromeritics) apparatus. The pore size distribution was determined by the BJH method applied to the desorption branch of the N_2 isotherm. The interaction between lauric acid and nickel ions was characterized by FT-IR measurements. The size and location of Ni particles on the catalyst surface were confirmed by transmission electron microscopy (TEM, Joel, JXA-8900R and Philips CM 20) using an ultrasonically dispersed catalyst sample (in ethanol) deposited on a carbon grid.

Average Ni particle sizes were determined by the equation, $d = (\sum n_i d_i)/n_i$. For the calculation of the number of surface sites, metal dispersion (D_M) was calculated on the basis of following equation. Here, $N(S)$ and $N(T)$ represent the number of metal atoms on

surface and the total number of metal atoms in the catalyst, respectively.

$$D_M = \frac{N(S)}{N(T)}$$

By assuming that the shape of metal particles is sphere, particle size of volume–area average (d_{VA}) was calculated by the following equation. Here, a_M and v_M represent the surface density of metal atom and the volume density of metal, respectively.

$$d_{VA} = 6\left(\frac{\sum V_i}{\sum A_i}\right) = 6\left(\frac{v_{mi}N(T)}{a_{mi}N(S)}\right) = 6\left(\frac{v_M}{a_M}\right)\Big/ D_M$$

The volume density of metal is correlated with the atomic weight of metal (M_w) as $v_M = M_w/\rho N_A$. Here, M_w, ρ, and N_A represent the atomic weight of metal, metal density, and Avogadro number, respectively. For nickel, a_M is 6.49×10^{-20} m^2/Ni atom and ρ is 8.845 (g/cm^3).

The temperature-programmed reduction (TPR) measurements were carried out in a conventional flow system with a moisture trap connected to a TCD at temperatures ranging from room temperature to 900 °C with a heating rate of 10 °C/min. For the TPR measurements, a mixed stream of H_2 (2 mL/min) and N_2 (20 mL/min) was used for 0.1 g of catalyst sample.

Temperatures-programmed desorption (TPD) profile of *o*-dichlorobenzene from each catalyst was determined in a conventional flow system equipped with a TCD. Prior to the TPD experiment, each catalyst was reduced with a stream of H_2 at 550 °C for 6 h, and then it was cooled down to the adsorption temperature of 190 °C with an inert gas stream. Gas phase *o*-dichlorobenzene (5.2×10^{-2} mol) was fed to the catalyst for adsorption with a stream of N_2. The physically adsorbed *o*-dichlorobenzene was removed at 190 °C by evacuation at the pressure of 2×10^{-2} Torr. After cooling down to room temperature, the catalyst sample was heated up to 100 °C for 1 h. Temperature was then raised up to 800 °C with a ramping rate of 10 °C/min using He (10 mL/min) as a carrier gas for 0.3 g of catalyst sample.

2.3. Hydrodechlorination of o-dichlorobenzene (DCB)

Hydrodechlorination of *o*-dichlorobenzene was carried out in a continuous flow fixed-bed reactor at an atmospheric pressure. Each catalyst (0.2 g) with a size of 150–200 μm was charged into a tubular quartz reactor, and activated with a mixed stream of H_2 (20 mL/min) and N_2 (20 mL/min) at 550 °C for 6 h. The reaction temperature was maintained at 250–350 °C. *o*-Dichlorobenzene (8.2×10^{-3} mol/h) was sufficiently vaporized by passing a pre-heating zone and fed into the reactor. The products were periodically sampled, and analyzed with a GC-MS and a GC (HP 5890 II, FID).

3. Results and discussion

3.1. Interaction between lauric acid and nickel ions

In order to investigate the interaction between lauric acid and nickel ions, FT-IR measurements were conducted for lauric acid and nickel precursor–lauric acid micelle complex. As shown in figure 2, the spectrum of lauric acid showed a strong band at 1700 cm^{-1} assigned to the carboxyl group of lauric acid, while the spectrum of micelle complex sample exhibited two distinct bands at 1335–1440 and 1550–1650 cm^{-1} assigned to symmetric $-COO^-$ stretching and asymmetric $-COO^-$ stretching bands, respectively. This result indicates that the carboxyl group of lauric acid was transformed into a carboxylic salt with nickel ions, resulting from the interaction of lauric acid and nickel ions.

3.2. XRD analyses

Figure 3(a) shows the XRD patterns of supported Ni catalysts calcined at 550 °C. The XRD patterns of two Ni–alumina catalysts were similar to the XRD pattern of mesoporous alumina (MA) support calcined at 550 °C. The NiAl-comp catalyst exhibited the characteristics peaks of nickel oxide, indicating the aggregation of nickel species. On the other hand, however, no peaks representing nickel oxide or metallic nickel were observed in both the Ni–alumina catalysts, indicating highly dispersed nickel species on the alumina supports [24,25]. It was revealed that the surfactant molecules (lauric acid) in the as-synthesized Ni–alumina interacted with nickel ions, leading to the formation of micelle complex composed of nickel ion and lauric acid. It is likely that the interaction between nickel ions and sur-

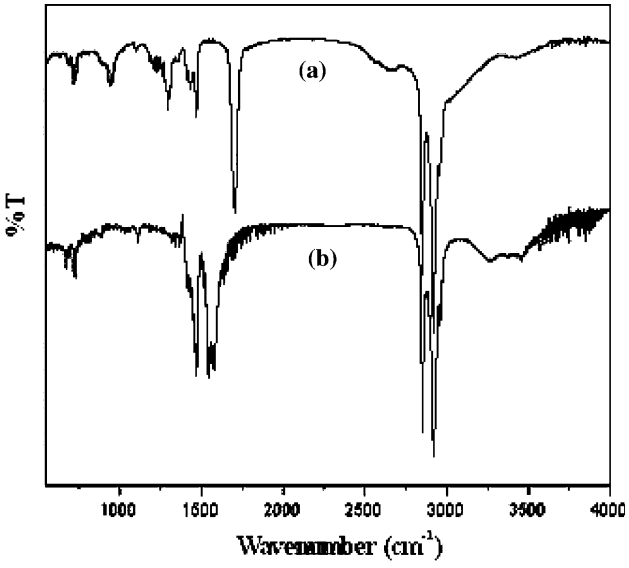

Figure 2. FT-IR spectra of (a) lauric acid and (b) nickel precursor–lauric acid micelle complex.

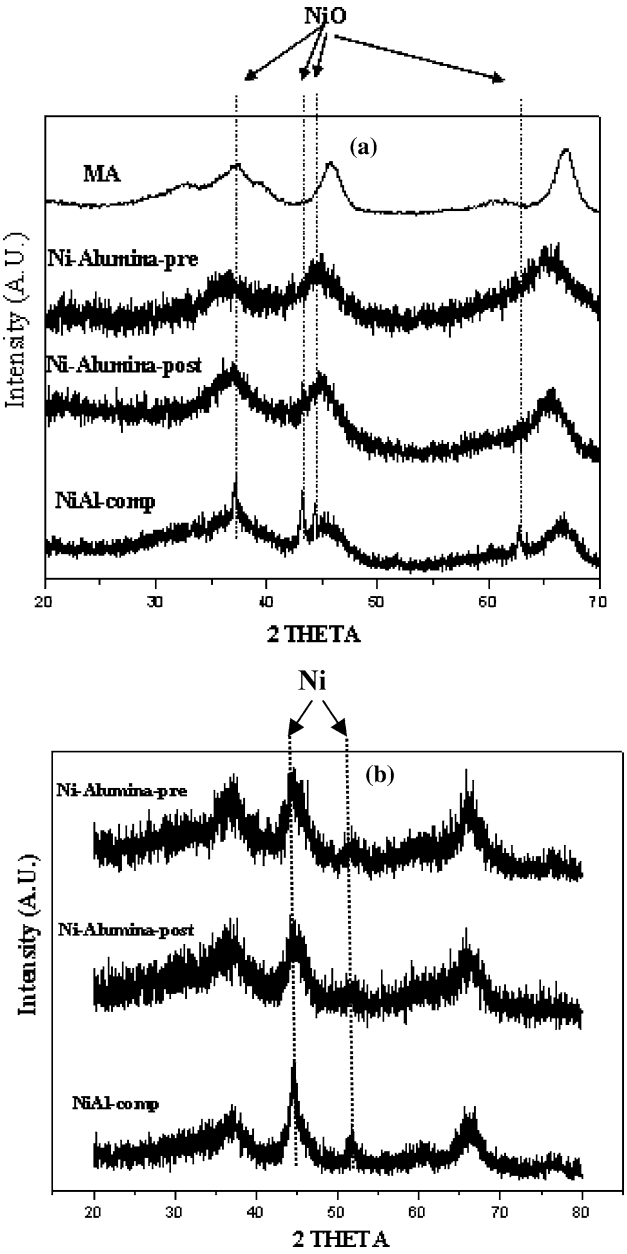

Figure 3. XRD patterns of supported Ni catalysts (a) calcined and (b) reduced at 550 °C. XRD pattern of pure mesoporous alumina (MA) was presented for comparison purpose.

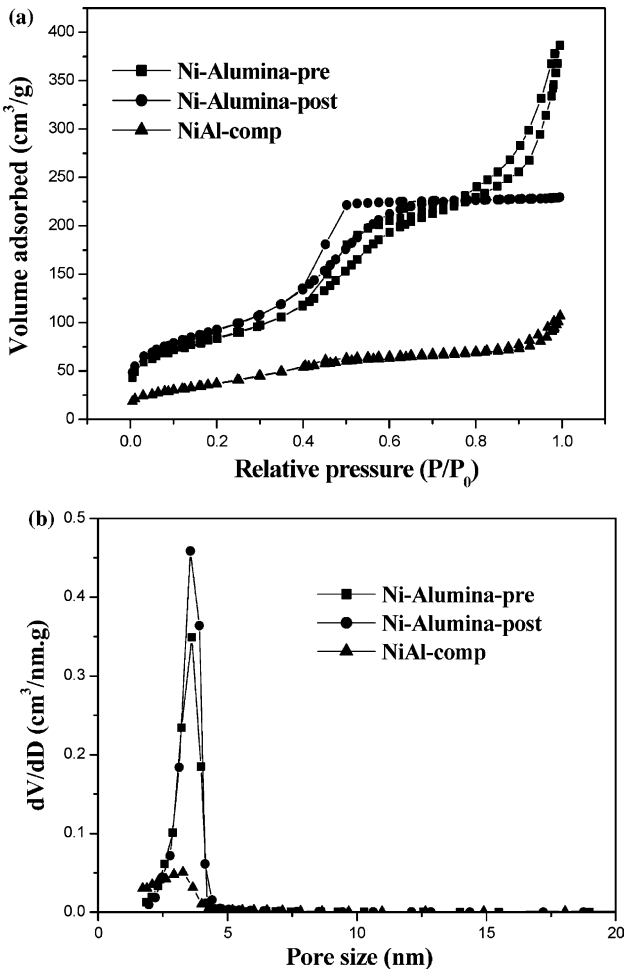

Figure 4. (a) N_2 adsorption–desorption isotherms and (b) pore size distributions of supported Ni catalysts.

factant molecules favorably served for the dispersion of nickel species on the alumina support. There was no such an interaction in the NiAl-comp catalyst, which resulted in large nickel oxides on the alumina support. In the XRD patterns of reduced catalysts (figure 3(b)), the characteristic peaks for metallic nickel were observed in all cases. Compared to the Ni–alumina catalysts, the NiAl-comp catalyst showed sharp and intense peaks for metallic nickel. This indicates that the NiAl-comp catalyst retained larger nickel crystallites than the Ni–alumina catalysts. It is believed that the strong interaction between nickel species and alumina support in the Ni–alumina catalysts resulted in the formation of small metallic nickel particles upon reduction.

3.3. *Investigation of textural properties by N_2 sorption and SAXS*

Figure 4 shows the nitrogen adsorption–desorption isotherms and pore size distributions of supported Ni catalysts. All the catalysts examined in this work exhibited typical type IV isotherms with H2 hysteresis loops. Both the Ni–alumina catalysts showed narrow pore size distribution centered at ca. 4 nm, while the NiAl-comp catalyst exhibited a very small peak of pore size distribution centered at ca 3.2 nm, implying the absence of templating effect in the NiAl-comp catalyst. It is noticeable that the shapes of isotherms of Ni–alumina catalysts were slightly different from each other. Both the Ni–alumina catalysts showed a capillary condensation at a relative pressure of 0.4–0.5. This is one of the typical characteristics of mesoporous materials, indicating the existence of structural mesoporosity (framework mesoporosity). However, an extra large adsorption at relative pressure above 0.8 was observed only for Ni–alumina-pre catalyst. This additional

adsorption may be attributed to the filling of textural mesopores, resulting from the intergrowth or aggregation of primary nanoparticles [30–32].

Detailed characterization results of the supported catalysts are listed in table 1. The Ni–alumina catalysts prepared with lauric acid as a template were found to have relatively high surface area with large pore volume, while the NiAl-comp catalyst retained inferior textural properties due to non-templating effect. It should be noted that the value of V_{text}/V_{meso}, an index of textural porosity [30], was higher in the Ni–alumina-pre catalyst than in the Ni–alumina-post catalyst. It is likely that such differences in textural porosity between two Ni–alumina catalysts were closely related to the synthesis condition. As mentioned earlier, the hydrolysis of aluminum source was done under the presence of micelle complex comprising nickel ions and lauric acid in the preparation of Ni–alumina-post catalyst, while aluminum source was hydrolyzed before addition to the solution of micelle complex in the preparation of Ni–alumina-pre catalyst. The aluminum source employed in this work would readily react with water, causing fast hydrolysis and condensation reaction [33]. In the synthesis of Ni–alumina-post catalyst, aluminum source was hydrolyzed in presence of metal ions with corresponding counter anion, which retarded the reaction of aluminum source with water, leading to relatively slower hydrolysis rate than condensation rate. It was well known that slow hydrolysis rate resulted in the formation of highly networked structure [33]. On the contrary, fast hydrolysis rate was favorable for the formation of aggregates composed of primary particles, producing enhanced textural porosity [33]. In the synthesis of Ni–alumina-pre catalyst, the hydrolysis rate of aluminum alkoxide was much faster than the condensation reaction because the aluminum source was pre-hydrolyzed before mixing with the solution containing micelle complex.

The pore structures of mesoporous alumina and supported Ni catalysts were examined by small angle X-ray scattering (SAXS) measurements (although these are not shown here). The SAXS patterns exhibited only one peak at 0.5–3°, indicating well-organized pore structure without long-range orderness [34,35]. Furthermore, the SAXS intensity of the supported Ni catalysts was weaker than that of pure mesoporous alumina support. According to the literature [24,36], the generation of X-ray peaks resulted from a difference in the scattering power (or scattering contrast) between two building blocks (amorphous wall and channel) of mesoporous materials. Therefore, it is likely that the introduction of Ni particles onto alumina support gave rise to a weak X-ray peak.

3.4. Pore structure and metal particle size

Textural property and nickel particle size of the supported catalysts were investigated by transmission electron microscopy (TEM) analyses. Figure 5 shows the TEM images of supported Ni catalysts reduced at 550 °C. Except for NiAl-comp catalyst, pores of the Ni–alumina catalysts had a wormhole or sponge-like appearance indicative of a highly interconnected pore system [24,25]. High textural porosity arising from the contact of interparticles could be observed in the image of Ni–alumina-pre catalyst, while well-developed framework porosity was observed in the Ni–alumina-post catalyst, in good agreement with the N_2 adsorption–desorption results. Finely dispersed Ni–particles were found in both the Ni–alumina catalysts. The sizes of nickel particles showed no great difference in both the Ni–alumina catalysts. On the other hand, relatively larger metal particles with somewhat broad size distribution were observed in the NiAl-comp catalyst. This result indicates that the interaction between surfactant molecules and nickel ions favorably served for the dispersion of nickel particles in the Ni–alumina catalysts. From these results, it is expected that the Ni–alumina catalysts with high metal dispersion may show better catalytic performance than the NiAl-comp catalyst.

3.5. Investigation of reducibility by TPR

TPR experiments were carried out in order to investigate the reducibility of nickel species and the metal–support interactions [37–42]. Figure 6 shows the reduction profiles of supported nickel catalysts calcined at 550 °C. It is known that nickel catalysts supported on alumina showed different reduction patterns depending on the nature of interaction between nickel oxide and alumina support. Bulk nickel oxide, which does not interact with support, is reduced at around 400 °C.

Table 1
Physical properties of supported Ni catalysts prepared with (Ni–alumina catalysts) and without (NiAl-comp catalyst) surfactant

Sample	Nickel loading (wt%)[a]	Particle size (nm)	Dispersion (%)	S_{BET} (m^2/g)	V_p (cm^3g^{-1})[b]	V_{text}/V^c_{meso}
Ni–alumina-pre	12.3	5.2	19.7	303	0.60	1.5
Ni–alumina-post	12.5	6.8	15	331	0.36	0.33
NiAl-comp	11.8	12.3	8.3	136	0.16	0.77

[a]Nickel loading measured by ICP-AES.
[b]Pore volume obtained from nitrogen adsorption at $P/P_0 = 0.99$.
[c]V_{meso}: Framework pore volume obtained from nitrogen adsorption at $P/P_0 = 0.5$ ($V_{text} = V_p - V_{meso}$.)

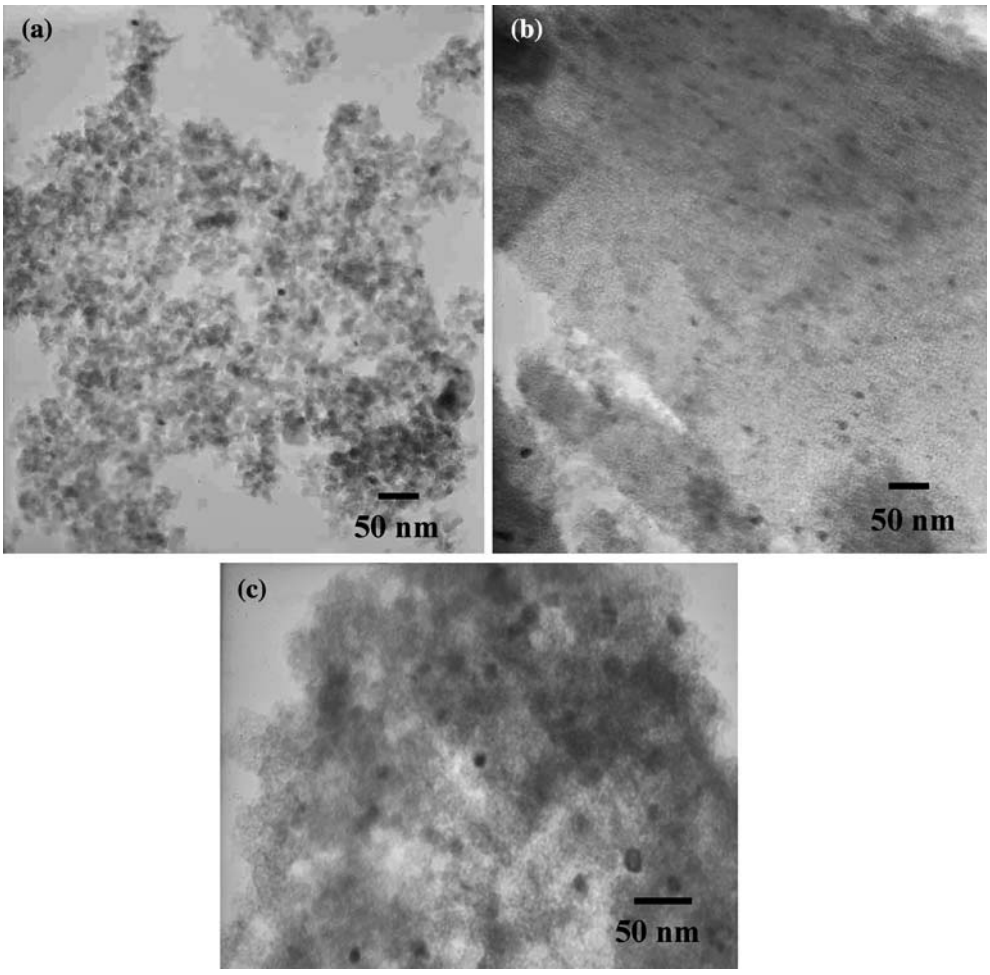

Figure 5. TEM images of reduced (a) Ni–alumina-pre, (b) Ni–alumina-post, and (c) NiAl-comp catalysts.

When the nickel species is supported on γ-Al_2O_3, the interaction between metal and support decreases the susceptibility for nickel ions to be reduced to metallic nickel and its reduction peak appears within a temperature window of 500–700 °C. The reduction profile of the Ni–alumina-pre catalyst could be divided into two regions. The peak at around 630 °C can be assigned to the typical reduction peak of Ni^{2+} that strongly interacts strongly with γ-Al_2O_3. The second peak at around 780 °C can be assigned to the reduction peak of nickel aluminate-like species. On the other hand, the Ni–alumina-post catalyst exhibited only one reduction peak at 710 °C, higher temperature than the first reduction peak temperature (630 °C) of the Ni–alumina-pre catalyst. This indicates that the Ni–alumina-post catalyst had less reducible Ni species, resulting from stronger interaction between Ni species and alumina. It is inferred that the reducibility of the supported Ni catalysts was affected by the catalyst preparation method. The preparation condition for the Ni–alumina-post, where the hydrolysis of aluminum source was conducted under the existence of micelle complex comprising lauric acid and nickel ion, which in turn made more homogeneous composite of nickel species and alumina component, would cause strong interaction between Ni species and alumina support in the final supported Ni–alumina-post catalyst. Compared to the Ni–alumina catalysts, the NiAl-comp catalyst showed more complicated reduction profile. The reduction profile could be divided into three regions. The first peak appearing at 430 °C, which was

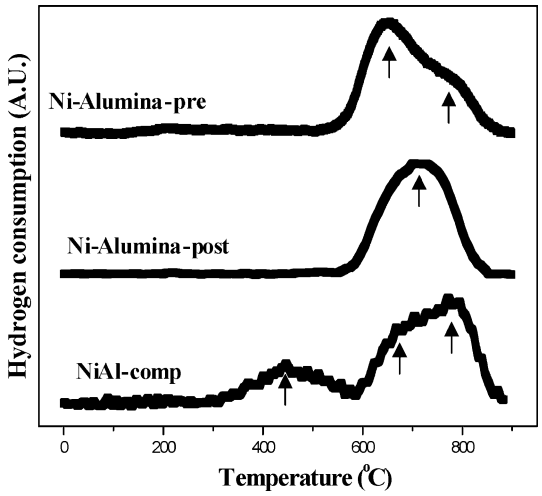

Figure 6. TPR patterns of Ni–alumina and NiAl-comp catalysts.

previously assigned to the bulk nickel oxide, might result from large nickel oxide aggregates as confirmed by XRD analysis. The second and third peaks can be attributed to the reduction of nickel species (Ni^{2+}) supported on γ-Al_2O_3 and nickel aluminate-like species, respectively. The complicated reduction profile of the NiAl-comp catalyst reflects the existence of the nickel species that differently interacted with alumina support, that is, existence of inhomogeneous mixture of nickel species and alumina component, causing relatively low dispersion of nickel species. Together with N_2 adsorption–desorption results, these results imply that the surfactant molecules played an important role in enhancing the porosity of supported Ni catalysts and the dispersion of nickel species as well.

3.6. Hydrodechlorination of o-dichlorobenzene (DCB)

It is known that two chlorines in the aromatic ring are removed sequentially or simultaneously in the hydrodechlorination [43]. The sequential elimination of chlorine involves hydrodechlorination of *o*-dichlorobenzene into chlorobenzene, and subsequent elimination of chlorine from chlorobenzene into benzene. On the other hand, the simultaneous removal of chlorine *via* hydrodechlorination results in the direct formation of benzene from *o*-dichlorobenzene.

Hydrodechlorination of DCB over the supported Ni catalysts produced HCl, chlorobenzene and benzene. It should be noted that products such as cyclohexane and chlorocyclohexane resulted from hydrogenation of aromatic compounds were not observed in this work. This is due to the fact that a dechlorinated product is immediately desorbed from the catalyst surface, and the activation energy over Ni catalyst is not sufficient for disruption of the resonance of aromatic ring [44]. Typical catalytic performance of the supported Ni catalysts in the hydrodechlorination of DCB is summarized in table 2. DCB conversion and benzene selectivity over all catalysts increased with increasing reaction temperature. In addition, the benzene selectivity was proportional to the DCB conversion. This trend of catalytic performance was a typical one in the hydrodechlorination of chlorinated aromatic compound over the supported Ni catalyst [44–49]. In the whole reaction temperature windows examined in this work, the NiAl-comp exhibited the lowest catalytic performance. As described previously, the NiAl-comp catalyst was in a state of inhomogeneous mixture of nickel species and alumina component, resulting in large agglomerates of nickel oxide. Therefore, the lowest metal dispersion can be expected in the NiAl-comp catalyst. Support structure may also affect the catalytic performance of the supported Ni catalysts. Cesteros *et al.* who tested Ni/Al-MCM-41 in the hydrodechlorination of 1,2,4-trichlorobenzene claimed that the enhanced distribution of nickel particles resulted from the favorable support structure was responsible for high activity of Ni/Al-MCM-41 [44]. Therefore, it is believed that the poor catalytic performance of the NiAl-comp catalyst was also attributed to its inferior pore structure.

Table 2
Catalytic performance of supported Ni catalysts in the hydrodechlorination of *o*-dichlorobenzene (DCB)

Catalyst	Temperature (°C)	Conversion (%)[a]	Benzene selectivity (%)[a]
Ni–alumina-pre	250	39	33
	300	54	48
	350	71	68
Ni–alumina-post	250	28	30
	300	43	41
	350	56	59
NiAl-comp	250	17	25
	300	27	33
	350	48	51

[a] *o*-Dichlorobenzene conversion and benzene selectivity obtained after 12-h reaction.

The Ni–alumina-pre catalyst showed the higher DCB conversion than the Ni–alumina-post catalyst. The difference in DCB conversion between two catalysts can be understood by TPR (before and after reduction) and DCB-TPD results, as summarized in table 3. Clearly, the degree of reduction of the Ni–alumina-pre catalyst is much higher than that of the Ni–alumina-post catalyst, indicating that the former catalyst can be reduced more easily at the catalyst activation step than the latter catalyst [5]. Figure 7 shows the DCB-TPD profiles of the Ni–alumina catalysts. Only single broad peak was observed for both catalysts. The peak area of TPD profile, which is equivalent to the amounts of DCB adsorbed on the catalyst, is closely related to the degree of reduction. It is clear that the Ni–alumina-pre catalyst adsorbed much more amounts of DCB than the Ni–alumina-post catalyst, indicating that the Ni–alumina-pre catalyst retained much more active sites for the hydrodechlorination than the Ni–alumina-post catalyst. Although the particle size of active metal may also affect the amounts of DCB adsorption, the difference in particle size between two catalysts was not significant (table 1). Therefore, it is believed that the amounts of DCB adsorption rather than the metal particle size are more closely related to the reducibility of the catalyst. Furthermore, it can be inferred that superior textural porosity of Ni–alumina-pre catalyst is partly responsible for the enhanced catalytic performance in the hydrodechlorination of DCB.

4. Conclusions

Mesoporous Ni–alumina catalysts were synthesized using aluminum alkoxide as a framework source and using a complex of nickel ion and lauric acid as a

Table 3
Analyses of peak area and area ratio of TPR (before and after reduction) and DCB-TPD results

Catalyst	A_1 (A.U.)	A_2 (A.U.)	A_3 (%)	$A_{3Ni\text{-}pre}/A_{3Ni\text{-}post}$	A_4 (A.U.)	$A_{4Ni\text{-}pre}/A_{4Ni\text{-}post}$
Ni–alumina-pre	43.9	28.7	34.6	1.45	19.6	1.59
Ni–alumina-post	43.1	32.8	23.8		12.3	

A_1: Peak area of TPR profile before reduction.
A_2: Peak area of TPR profile after reduction at 550 °C.
A_3: Defined as $(A_1-A_2)/A_1$ (degree of reduction).
A_4: Peak area of DCB-TPD profile.

template with metal source. When the hydrolysis was conducted under the presence of micelle complex, the resulting catalyst (Ni–alumina-post) exhibited well-developed framework porosity. A catalyst with enhanced textural porosity (Ni–alumina-pre) could be also prepared by hydrolyzing aluminum source before mixing with micelle complex. Both the Ni–alumina catalysts showed relatively high surface area with narrow pore size distribution centered at ca. 4 nm. Compared to the NiAl-comp catalyst that was synthesized without surfactant molecules, the Ni–alumina catalysts exhibited higher metal dispersion. Thus surfactant molecules played a favorable role in enhancing metal dispersion in the Ni–alumina catalysts. It was also revealed that the synthesis condition affected the catalyst reducibility and the textural porosity of the Ni–alumina catalysts. The Ni–alumina-post catalyst exhibited stronger interaction between metal and alumina support than the alumina-pre catalyst, leading to less reducible nickel species in the Ni–alumina-post catalyst. In the hydrodechlorination of *o*-dichlorobenzene (DCB), the NiAl-comp catalyst showed the lowest catalytic performance, which was attributed to the lowest metal dispersion. It was found that the degree of reduction at the activation temperature, which was closely related to the active sites for the hydrodechlorination of DCB, strongly affected the catalytic performance. The Ni–alumina-pre catalyst with higher degree of reduction showed better catalytic performance than the Ni–alumina-post catalyst. It was also believed that the textural porosity of Ni–alumina-pre catalyst was partly responsible for its enhanced catalytic performance.

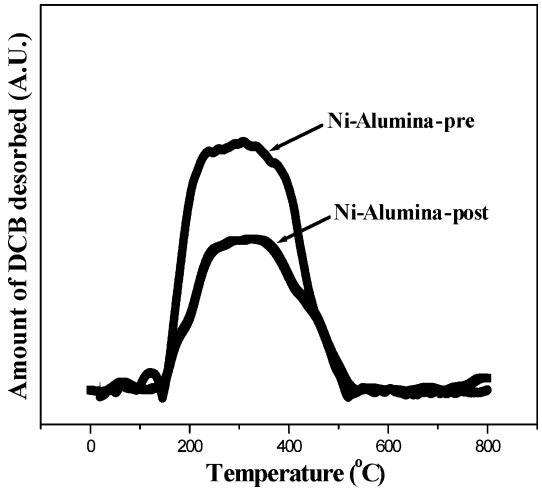

Figure 7. DCB-TPD profiles of Ni–alumina catalysts.

Acknowledgements

This work was supported by National Research Laboratory (NRL) program of the Korea Science and Engineering Foundation (KOSEF) and this research was conducted through the Engineering Research Institute (ERI) at Seoul National University, Korea.

References

[1] Z. Konya, V.F. Puntes, I. Kiricsi, J. Zhu, P. Alivisatos and G.A. Somorjai, Catal. Lett. 81 (2002) 137.
[2] Y.-M. Liu, Y. Cao, S.-R. Yan, W.-L. Dai and K.-N. Fan, Catal. Lett. 88 (2003) 61.
[3] D.-W. Park, S.-D. Choi, S.-J. Choi, C.-Y. Lee and G.-J. Kim, Catal. Lett. 78 (2002) 145.
[4] L.-X. Dai, K. Koyama and T. Tatsumi, Catal. Lett. 53 (1998) 211.
[5] P. Kim, Y. Kim, C. Kim, H. Kim, Y. Park, J.H. Lee, I.K. Song and J. Yi, Catal. Lett. 89 (2003) 185.
[6] K.-K. Kang, C.-H. Park and W.-S. Ahn, Catal. Lett. 59 (1999) 45.
[7] Y.S. Cho, J.C. Park, W.Y. Lee and J. Yi, Catal. Lett. 81 (2002) 89.
[8] Y. Liu, W. Zhang and T.J. Pinnavaia, Angew. Chem. Int. Ed. 40 (2001) 1225.
[9] Z. Zhang, Y. Han, L. Zhu, R. Wang, Y. Yu, S. Qiu, D. Zhao and F.S. Xiao, Angew. Chem. Int. Ed. 40 (2001) 1258.
[10] Y. Kim, P. Kim, C. Kim and J. Yi, J. Mater. Chem. 13 (2003) 2353.
[11] Y. Kim, C. Kim, J.W. Choi, P. Kim and J. Yi, Stud. Surf. Sci. Catal. 146 (2003) 209.
[12] J.C. Park, J.H. Lee, P. Kim and J. Yi, Stud. Surf. Sci. Catal. 146 (2003) 109.
[13] Y. Park, T. Kang, Y.S. Cho, J.C. Park, P. Kim and J. Yi, Stud. Surf. Sci. Catal. 146 (2003) 637.
[14] S. Cabrera, J.E. Haskouri, J. Alamo, A. Beltran, S. Mendioroz, M.D. Marcos and P. Amoros, Adv. Mater. 11 (1999) 379.
[15] S.B. Pu, J.B. Kim, M. Seno and T. Inui, Micro. Mater. 10 (1997) 25.
[16] F. Vaudry, S. Khodabandeh and M.E. Davis, Chem. Mater. 8 (1996) 1451.
[17] K.A. Koyano and T. Tatsumi, Micro. Mater. 10 (1997) 259.
[18] M. Yada, M. Machida and T. Kijima, Chem. Commun. 6 (1996) 769.
[19] S.A. Bagshaw and T.J. Pinnavaia, Angew. Chem. Int. Ed. 35 (1996) 1102.

[20] N. Yao, G. Xiong, Y. Zhang, M. He and W. Yang, Catal. Today 68 (2001) 97.
[21] J. Cejka, Appl. Catal. A 254 (2003) 327.
[22] X. Zhang, F. Zhang and K.-Y. Chan, Mater. Lett. 58 (2004) 2782.
[23] T. Oikawa, T. Ookoshi, T. Tanaka, T. Yamamoto and M. Onaka, Micro. Meso. Mater. 74 (2004) 93.
[24] P. Kim, Y. Kim, H. Kim, I.K. Song and J. Yi, J. Mol. Catal. A 219 (2004) 87.
[25] P. Kim, Y. Kim, H. Kim, I.K. Song and J. Yi, Appl. Catal. A 272 (2004) 157.
[26] S. Shio, A. Kimura, M. Yanaguchi, K. Yoshida and K. Kuroda, *Chem. Commun.* (1998) 2461.
[27] X. Wang, T. Dou and Y. Xiao, *Chem. Commun.* (1998) 1053.
[28] E. Matijevic, Chem. Mater. 5 (1993) 412.
[29] H.P. Lin and C.P. Tsai, Chem. Lett. 32 (2003) 1092.
[30] M.-C. Chao, H.-P. Lin, C.-Y. Mou, B.-W. Cheng and C.-F. Cheng, Catal. Today 97 (2004) 81.
[31] T.R. Pauly, Y. Lin, T.J. Pannavaia, S.J. Billinge and T.P. Ricker, J. Am. Chem. Soc. 12 (1999) 8835.
[32] F. Rouquerol, J. Rouquerol and K. Sing, *Adsorption by Powders and Porous Solid.* (Academic Press, London, 1999).
[33] C.J. Brinker and G.W. Scherer, *Sol–Gel Science: The Physics and Chemistry of Sol–Gel Processing* (Academic Press, London, 1990).
[34] V.I. Parvulescu, H. Bonnemann, V. Parvulescu, U. Endruschat, A. Rufinska, W. Lehmann, B. Tesche and G. Poncelet, Appl. Catal. A 214 (2001) 273.
[35] W. Deng, P. Bodart, M. Pruski and B.H. Shanks, Micro. Meso. Mater. 52 (2002) 169.
[36] B. Marler, U. Oberhangemann, S. Vortmann and H. Gies, Micro. Mater. 6 (1996) 375.
[37] J. Zielinski, J. Catal. 76 (1982) 157.
[38] G.R. Gavalas, C. Phichitkul and G.E. Voecks, J. Catal. 88 (1984) 54.
[39] P.K. De Bokx, W.B.A. Wassenberg and J.W. Geus, J. Catal. 104 (1987) 86.
[40] J.M. Rynkowski, T. Paryjczak and M. Lenik, Appl. Catal. A 106 (1992) 73.
[41] O. Dewaele and G.F. Froment, J. Catal. 184 (1999) 499.
[42] B.W. Hoffer, A.D. Langeveld, J.P. Janssens, R.L.C. Bonne, C.M. Lok and J.A. Moulijn, J. Catal. 192 (2000) 432.
[43] J. Frimmel and M. Zdrazil, J. Catal. 167 (1997) 286.
[44] Y. Cesteros, P. Salagre, F. Medina and J.E. Sueiras, Catal. Lett. 79 (2002) 83.
[45] M.A. Keane, G. Pina and G. Tavoularis, Appl. Catal. B 48 (2004) 275.
[46] Y. Cesteros, P. Salagre, F. Medina and J.E. Sueiras, Catal. Lett. 67 (2000) 147.
[47] K.V. Murthy, P.M. Patterson, G. Jacobs, B.H. Davis and M.A. Keane, J. Catal. 223 (2004) 74.
[48] Y. Cesteros, P. Salagre, F. Medina, J.E. Sueiras, D. Tichit and B. Coq, Appl. Catal. B 32 (2001) 25.
[49] Y. Cesteros, P. Salagre, F. Medina and J.E. Sueiras, Appl. Catal. B 25 (2000) 213.